Phase behavior of two-dimensional Brownian systems of corner-rounded hexagons

Zhanglin Hou,[1,*] Kun Zhao,[1,*,†] Yiwu Zong,[1] and Thomas G. Mason[2,3,‡]

[1]*Key Laboratory of Systems Bioengineering (Ministry of Education), School of Chemical Engineering and Technology, Tianjin University, Tianjin 300072, People's Republic of China*

[2]*Department of Physics and Astronomy, University of California Los Angeles, Los Angeles, California 90095, USA*

[3]*Department of Chemistry and Biochemistry, University of California Los Angeles, Los Angeles, California 90095, USA*

(Received 26 October 2018; published 2 January 2019)

Investigations into the phase behavior of Brownian systems of nonspherical colloids have received considerable attention because these systems can exhibit very rich self-assembled structures, some of which have potential for applications. In this work, we explore the phase behavior of corner-rounded hexagons in two dimensions, both through experiments and Monte Carlo (MC) simulations. Our experiments, using lithographically shape-designed hexagons, which have corner-rounded vertices and nearly hard in-plane interactions, reveal three different solid phases for increasing particle area fraction ϕ_A: hexagonal rotator crystal (RX), hexagonal crystal (HX), and frustrated hexagonal crystal (FHX). In the RX phase, hexagons form a hexagonal lattice, but they are randomly oriented and their rotations are ergodic. In the HX phase, hexagons orient uniformly on average, but their rotations are still ergodic via slower hopping motion. In the FHX phase, all hexagons are uniformly oriented, but their rotations are highly bound and nonergodic. MC simulation results on matching rounded hexagons confirm this experimentally observed sequence of phases. Using simulations, we increase the corner roundness and show that the molecular-orientational order decreases at fixed ϕ_A. Our results provide insights into controlling the large-scale self-assembly of spatially and orientationally ordered two-dimensional arrays of colloids through particle shape design and crowding conditions.

DOI: 10.1103/PhysRevMaterials.3.015601

I. INTRODUCTION

Colloidal self-assembly is being studied extensively due to its broad applications in fabricating new functional soft materials [1–4]. Self-assembled structures of Brownian colloidal systems are controlled by the phase behavior of constituent colloids, which depends on many factors, such as shapes [4,5], charges [6], magnetic properties [7], or roughness [8,9] of particles that can influence interparticle interactions [10]. Two-dimensional (2D) colloidal systems with hard particle interactions have attracted particular attention since their phase behavior is determined solely by the shapes of constituent colloids and the entropy of these systems.

When slowly crowded, Brownian systems of simple discotic colloids form an intermediate liquid crystalline 'hexatic' (H) phase, which has short-range positional order and quasi-long-range bond-orientational order, before crystallizing into a solid. Recent simulations of hard disks have concluded that the 2D melting transition of the hard disk system is a two-step process via a H phase, and the solid-hexatic phase transition is continuous while the hexatic-liquid phase transition is weakly first order [11,12], unlike the first-order liquid-to-crystal transition of hard spheres in 3D [10]. This is different from the well-known Kosterlitz-Thouless-Halperin-Nelson-Young (KTHNY) theory that has predicted a similar two-step melting scenario in 2D via a hexatic phase, but with both continuous solid-hexatic and continuous hexatic-liquid transitions [13–15].

Compared with disks, anisotropic colloids in 2D such as rods, triangles, squares, pentagons, and rhombs exhibit much richer phase behavior [1]. For example, depending on their aspect ratios, 2D hard rods can display either an isotropic-nematic-solid phase sequence or an isotropic-solid phase sequence as the particle area fraction ϕ_A increases [16]. Brownian 2D systems of anisotropic colloids have been the focus of much work, including both experiments and simulations [16–33]. Experimental research on colloids was initially limited to few available anisotropic shapes, such as tobacco mosaic virus [34], but huge progress has been made in the last two decades on new fabrication techniques for shape-designed colloids [35]. In particular, photolithographic techniques have been applied to fabricate colloidal platelets with a wide range of complex 2D shapes that are small enough for entropic Brownian excitations to dominate [36–38]. Using this technique, many anisotropic platelets such as triangles, squares, pentagons, rhombs, and concave-shaped square cross colloids have been made and their phase behavior in 2D have been studied [26–29,31]. For instance, the Brownian triangle system has been shown to form a new 'triatic' liquid crystal phase, rather than crystallize, when slowly crowded [28]. By contrast, two crystal phases, a hexagonal rotator crystal (RX) and rhombic crystal (RB), have been observed in a crowded system of Brownian squares [27]. Although the fivefold symmetry of regular pentagons is incommensurate with common 2D crystal symmetries, as ϕ_A is progressively increased, the pentagon system first goes through a liquid-RX

*These authors contributed equally to this work.
†Corresponding author: kunzhao@tju.edu.cn
‡Corresponding author: mason@chem.ucla.edu

phase transition yielding a sixfold crystal, and then a transition from RX to a frustrated hexagonal rotator crystal (FRX), in which the rotation of pentagons is frozen, has been observed. At even higher ϕ_A, pentagons form a frustrated rotator glass state, and the degree of spatial order in the system decreases [26]. Thus, symmetries of phases resulting from entropy maximization do not necessarily reflect the symmetries of the shapes of constituent particles.

Computer simulations by Monte Carlo (MC) and molecular dynamics (MD) methods are powerful tools that have been widely used to study the 2D phase behavior of anisotropic colloids [16–25] due to their relatively easier implementation and precise control over parameters such as aspect ratios, compared with experimental studies. Recently, Anderson *et al.* [24] have performed detailed MC simulations of monodisperse regular n polygons (for n ranging from 3 to 14), and found that when $n \geqslant 7$, regular polygons show a similar disklike phase behavior; whereas for regular hexagons, squares, and triangles, these systems follow KTHNY theory and melt through two-step continuous transitions from solids to liquids via hexatic or tetratic phases. When $n = 5$, the pentagon system exhibits a first-order melting transition. Both experimental [26–28] and simulation [24] results clearly show that the melting transition of 2D systems of regular polygons depends upon both particle shape and symmetry.

Among regular polygons, triangles, squares, and hexagons are the only shapes that can fully tile the plane. A regular hexagon, in particular, also has a sixfold symmetry which matches the symmetry of hexagonally close-packed structures. So, Brownian systems of regular hexagons present a special case that also deserves careful experimental attention. Simulations of a hexagon system display isotropic-hexatic-solid phase transitions as ϕ_A increases [24], but there has been no experimental report yet on either the phase diagram of hexagons or characterizing the solid phase in detail. Moreover, the phase behavior of anisotropic colloids can be extremely sensitive to smaller details of the colloidal shapes. For example, in a hard square system, MC simulation results show a liquid-tetratic-square crystal transition sequence [20], whereas experiments show a different sequence: liquid-hexagonal rotator crystal-rhombic crystal [27]. As suggested in the experimental work as a possible explanation for this difference, the observed difference is largely due to the corner rounding of squares used in experiments; this has later been confirmed by a detailed MC simulation [23]. Thus, a similar question arises for hexagonal platelets that have only hard interactions: how does the degree of corner rounding of vertices affect their phase behavior when crowded in the presence of Brownian excitations? To answer this, we first lithographically fabricate hexagonal platelets with edge length $L = 1.7 \pm 0.1\,\mu$m and thickness $1.4 \pm 0.1\,\mu$m. Due to the limited minimum feature size of the stepper photolithography used, which is primarily a result of optical diffraction of patterned UV light, the fabricated hexagons have rounded corners with a roundness $\zeta = 0.3$ [Figs. 1(a) and 1(b)]. We define the corner roundness parameter as $\zeta = R_0/R_{max}$, where R_0 is the radius of circle [green dashed circle in Fig. 1(a)] that is best superimposed on a rounded corner and the center of this circle lies on the line connecting that rounded corner and the center of the hexagon [red dashed line in Fig. 1(a)].

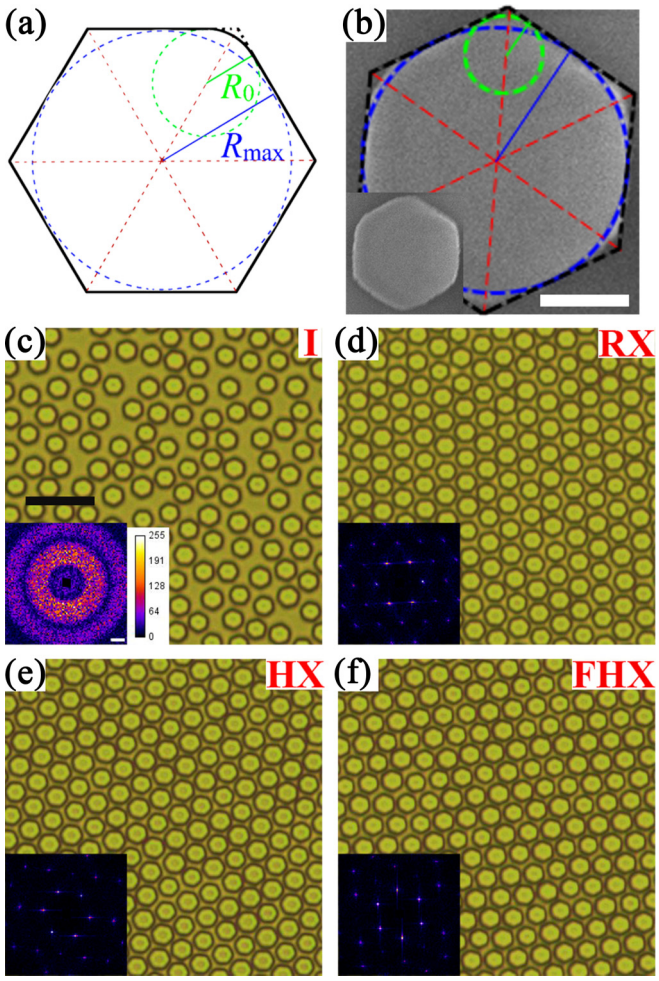

FIG. 1. Illustration of the definition of corner roundess ζ and micrographs of hexagons and their self-assembled structures. (a) ζ is defined as $\zeta = R_0/R_{max}$, where R_0 is the radius of the circle (green dashed circle) that is best superimposed on a rounded corner and the center of this circle lies on the line connecting that rounded corner and the center of the hexagon (red dashed line). $R_{max} = \sqrt{3}L/2$ is the radius of the inscribed circle (blue dashed circle) of the hexagon. Here, L is the edge length of the ideal unrounded hexagon. (b) A scanning electron microscopy (SEM) image of a hexagon with color lines superimposed to illustrate the measurement of ζ. The lower left inset shows the bare SEM image. Scale bar is 1 μm. (c)–(f) Transmission optical micrographs of a 2D Brownian system of lithographically fabricated hexagons at different particle area fractions ϕ_A: (c) 0.49, isotropic (I); (d) 0.64, hexagonal rotator crystal (RX); (e) 0.69, hexagonal crystal (HX); and (f) 0.72, frustrated hexagonal crystal (FHX), in which the rotation of particles is dynamically frozen. Lower-left insets: fast Fourier transform (FFT) intensities calculated from real-space images (scale bar is $0.2\,\mu m^{-1}$). FFTs have been rendered in pseudocolor to emphasize peak features. Black scale bar in (c) is 10 μm.

Here, $R_{max} = \sqrt{3}L/2$ is the radius of the inscribed circle [blue dashed circle in Fig. 1(a)] of the hexagon. We then experimentally study the phase behavior of slowly crowded 2D Brownian systems of these hexagons. We find three crystal phases in the solid region and characterize these phases in detail. Then, to understand the effect that corner rounding has

on the phase behavior of hexagons more broadly, we perform MC simulations on a series of hexagons with different corner roundness from $\zeta = 0$ up to $\zeta = 0.99$. After taking into account edge roughness and rescaling our simulation ϕ_A, we show that the sequence of phase transitions in simulations is consistent with our experimental observations at the same ζ.

II. EXPERIMENTAL AND SIMULATION METHODS

A. Preparation of samples

Equilateral hexagons with edge length $L = 1.7 \pm 0.1\ \mu$m and thickness $1.4 \pm 0.1\ \mu$m are fabricated from SU-8 polymer by 5x reduction stepper UV photolithography using a photomask containing many replicates of larger unrounded hexagons. Due to the stepper's limited feature size (≈300 nm), the corners of the hexagons are slightly rounded with roundness $\zeta \sim 0.3$. The size polydispersity of obtained hexagons is ∼6%. Following the same method as in Ref. [27], we have prepared a two-dimensional monolayer of hexagons in a rectangular optical cuvette ($0.2 \times 4.0 \times 20$ mm) using roughness-controlled depletion attractions (depletion agent: sulfate-stabilized polystyrene spheres, diameter ∼0.02 μm, concentration ∼0.5% w/v). Hexagons are then concentrated by tilting the cuvette about its long axis at angles between 1° and 6°, and a slowly varying spatial gradient in ϕ_A is developed. After waiting for a minimum of two months for equilibration, images at specific ϕ_A along the cuvette are taken under microscope. About 320 hexagons are observed in a single microscopic field of view ($64 \times 64\ \mu$m) at high ϕ_A.

B. Image analysis and measurement of area fraction

For each image, the center position and six vertices of each hexagon are determined by a customized software written in Interactive Data Language. Then the orientation of a hexagon is defined by the line from the center to one of its vertices. Because the time interval between recorded frames is small, i.e., about 0.071 s/frame, no very large rotations approaching $\pm\pi/6$ between two consecutive frames of any hexagon were observed at the tested ϕ_A. Thus, because our frame rate is high compared to the rotational diffusion rate, our tracking program effectively ensures that the same vertex of each hexagon, and thus its orientation, is followed throughout the entire movie. All values of ϕ_A are calculated using particle center locations, and the average measured size of the hexagons is determined by scanning electron microscopy. Because of nanoscale edge roughness of the hexagon particles that is not apparent in the optical micrographs, the effective area fractions of particles may be slightly larger than our reported values (i.e., values of ϕ_A may be up to about 6.8% larger as a consequence of edge roughness).

C. MC simulation methods

MC simulations of corner-rounded Brownian hexagons were performed using isothermal-isobaric *NPT* ensembles in a square box with periodic boundary conditions: $N = 3584$ particles are used. Both compression and expansion runs are performed. In each MC step, there are N particle trial moves (each particle will have a trial move once) and four box trial moves. In both particle and box trial moves, the acceptance ratio is set to be 40%. The simulation is first run 4.5×10^6 steps to equilibrate, and then run 0.5×10^6 steps to determine a statistical ensemble average. The Supplemental Material [39] provides more details of the methods and additional results.

III. RESULTS AND DISCUSSION

Optical micrographs of crowded Brownian hexagons after slowly raising ϕ_A are shown in Figs. 1(c)–1(f). At $\phi_A = 0.49$, the system is in an isotropic phase (I) [Fig. 1(c)]; the positions and orientations of hexagons are disordered and random. The Fourier transform (FT) of this image yields a symmetric ringlike pattern, which is typical for an isotropic disordered phase. For larger $\phi_A = 0.64$ [Fig. 1(d)], the system has solidified into a hexagonal rotator crystal phase (RX); the positions of hexagons are ordered in an equilateral hexagonal lattice (see inset), but the orientations of hexagons are still random. The corresponding FT shows a hexagonal pattern of sharp peaks. When ϕ_A is further increased to 0.69, the positions of hexagons form an ordered equilateral hexagonal lattice [see Fig. 1(e) and inset], but also their orientations become uniform (i.e., all edges of hexagons become strongly aligned with one of three axes in the plane), so the system is in a distinguishably different hexagonal crystal phase (HX). At an even higher $\phi_A = 0.72$ [Fig. 1(f)], hexagons are packed so tightly that rotational tip-tip passage between neighboring hexagons is rarely observed over very long timescales (e.g., days). So at this area fraction, the system is in a frustrated hexagonal crystal phase (FHX). Compared with the HX phase, the FHX phase is structurally the same but dynamically different. Because the symmetry of the hexagonal platelets matches that of the self-organized lattice structure, at even larger ϕ_A we do not observe an increase in disorder. This is different than observations for similar systems of regular pentagons that showed an increasing defect density when very strongly crowded [26] because such pentagons have a fivefold symmetric particle shape that is mismatched with the sixfold symmetry of the self-organized lattice.

To characterize the phase behavior of the experimental hexagon system quantitatively, we calculate relevant order parameters and correlation functions. The sixfold bond-orientational order Ψ_6, positional-order S_Δ, and molecular-orientational order Φ_6 parameters are $\Psi_6 e^{i\omega} = N^{-1}\sum_{j=1}^{N}\varphi_6(\vec{r}_j)$, $S_\Delta = N^{-1}|\sum_{j=1}^{N}\xi_6(\vec{r}_j)|$, and $\Phi_6 = N^{-1}|\sum_{j=1}^{N} e^{i6\theta_j}|$, respectively [27,40]. Here, ω represents a global phase; N is the total number of particles; $\varphi_6(\vec{r}_j) = N_j^{-1}\sum_{k=1}^{N_j} e^{i6\gamma_{jk}}$ is the local sixfold bond-orientational order parameter for particle j; $\vec{r}_j$ is the center position vector of particle j in lab frame, and γ_{jk} is the angle between an arbitrary fixed axis and the line connecting the centers of particles j and k. N_j is the number of nearest neighbors of particle j, obtained by a Voronoi construction using center positions of particles; $\xi_6(\vec{r}_j) = e^{i\vec{G}_6\cdot\vec{r}_j}$ is the positional order parameter for each particle j, $\vec{G}_6$ is the reciprocal lattice vector of the equilateral hexagonal lattice; and θ_j is the angle of "molecular" orientation of particle j. Correspondingly, the sixfold bond-orientational correlation function $g_6(r)$,

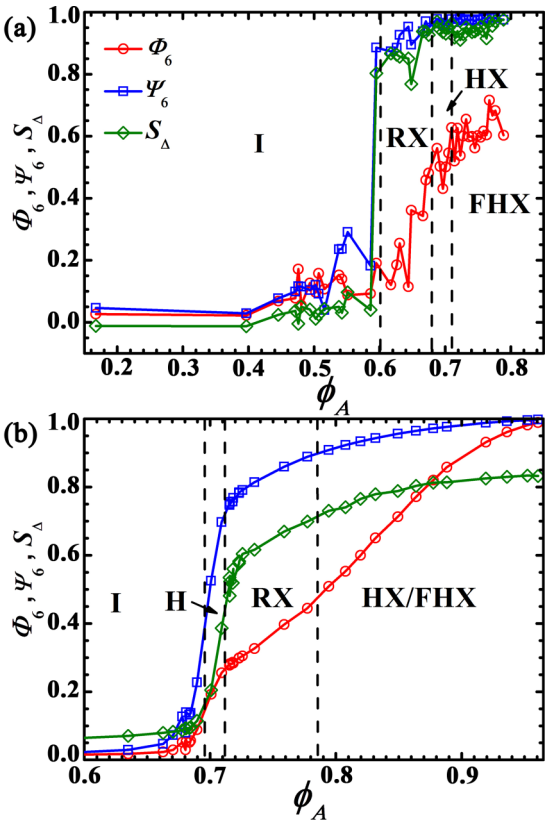

FIG. 2. Order parameters as a function of ϕ_A obtained from (a) experimental measurements and (b) Monte Carlo simulations with the same ζ as experimental hexagons ($\zeta = 0.3$). Red circles: molecular-orientational order Φ_6; blue squares: sixfold bond-orientational order Ψ_6; green diamonds: positional order S_Δ. The positional order S_Δ in (a) at low area fractions has been corrected by subtracting using an average of the first two points determined at low ϕ_A to offset the nonzero value of calculated S_Δ in the isotropic phase (necessary given the employed numerical method). The dashed lines indicate the estimated boundary of the phases.

the spatial correlation function relating to positional order ${g_6}^s(r)$, and the sixfold molecular-orientational correlation function ${g_6}^{\rm mo}(r)$, are defined as $g_6(r) = {\rm Re}\langle\varphi_6^*(0)\varphi_6(r)\rangle$, $g_6^s(r) = {\rm Re}\langle\xi_6^*(0)\xi_6(r)\rangle$, and $g_6^{mo}(r) = \langle\cos[6\theta(r) - 6\theta(0)]\rangle$, respectively.

In Figs. 2 and 3, we show and compare the results of these calculations for the experiment and for the corresponding MC simulation. From Fig. 2(a), for $\phi_A < 0.6$, we find that Ψ_6, S_Δ, and Φ_6 are all small, and the system is isotropic (I). The correlation functions in the I phase all decay quickly, indicating only short-range order (see Fig. 3). When $\phi_A \geqslant 0.6$, Ψ_6 and S_Δ both exhibit an abrupt and highly correlated increase. By contrast, Φ_6 does not increase to a high value (e.g. >0.5) until ϕ_A reaches ~0.68. So for $0.6 \leqslant \phi_A \leqslant 0.68$, the system is in a RX phase. As an example, at $\phi_A = 0.64$, $g_6(r)$ shows a strong correlation with no apparent decay within the measured range of r, and ${g_6}^s(r)$ shows an algebraic decay at large r with an exponent larger than $-1/3$, indicating that this phase is stable against a dislocation-mediated KTHNY transition [40]. However, ${g_6}^{\rm mo}(r)$ decays very quickly at $\phi_A = 0.64$. These results show that the RX phase has (quasi-)long-range bond-

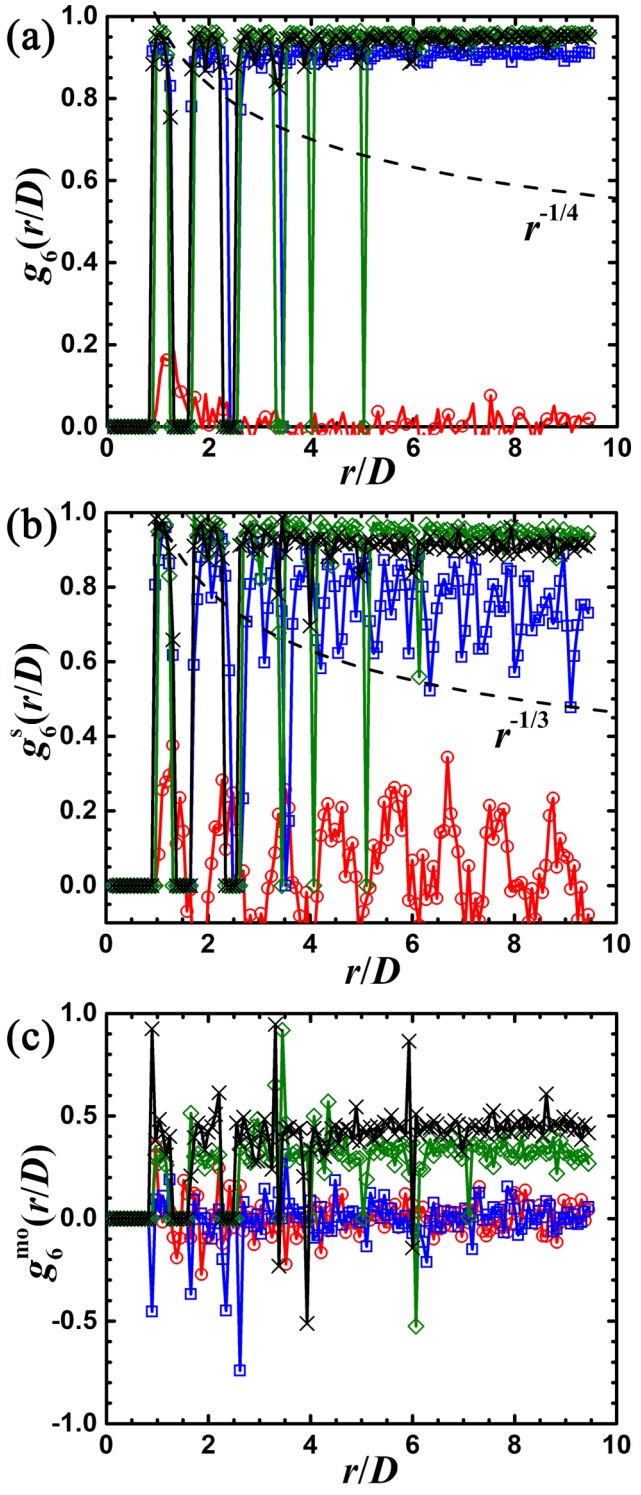

FIG. 3. Measured experimental correlation functions at different ϕ_A. (a) Sixfold bond-orientational correlation function $g_6(r)$. Dashed line is $\propto r^{-1/4}$, which is the KTHNY prediction for $g_6(r)$ at the H-I transition point. (b) Spatial correlation function $g_6^s(r)$. Dashed line is $\propto r^{-1/3}$, which is the KTHNY prediction for $g_6^s(r)$ at the crystal-hexatic transition point. (c) Sixfold molecular-orientational correlation function $g_6^{\rm mo}(r)$. $\phi_A = 0.49$ (red circles), 0.64 (blue squares), 0.69 (green diamonds) and 0.72 (black crosses). $D = 2L$ is the diameter of circumscribed circle of a regular hexagon. The large fluctuations of correlation functions in the crystal phase are a consequence of the crystalline order.

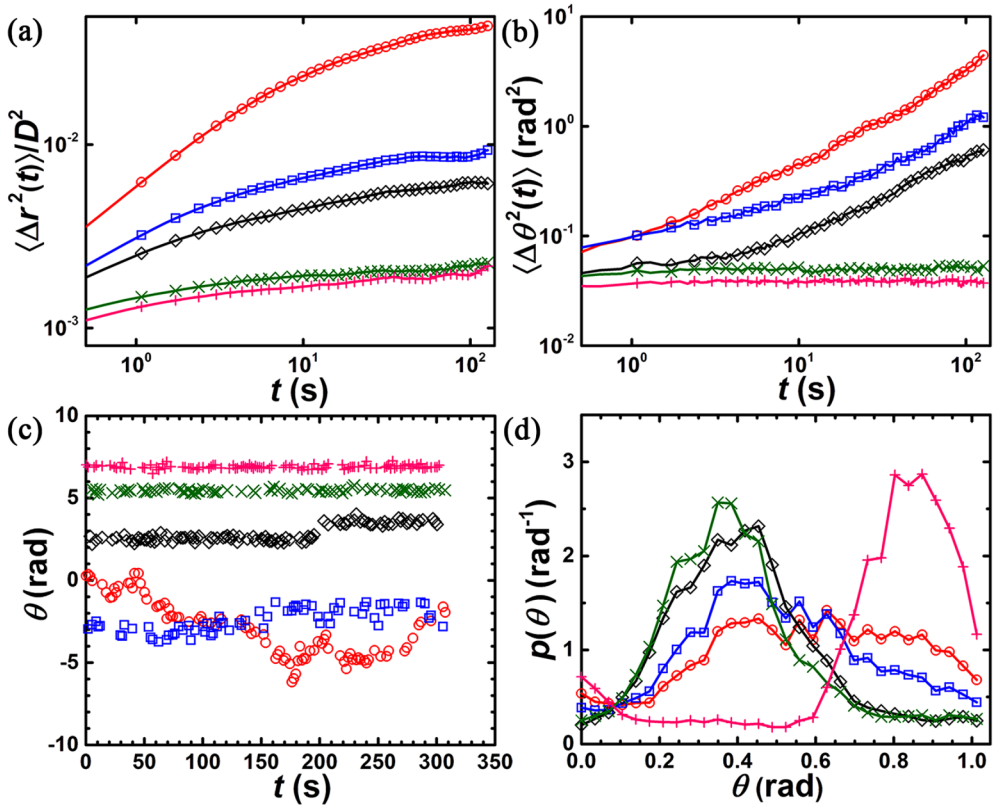

FIG. 4. Dynamics of hexagons at different ϕ_A. Time- and ensemble-averaged (a) MSD, (b) MSAD. (c) Examples of rotational trajectory of individual hexagons as a function of time t. Trajectories have been shifted upward for clarity. (d) Probability density of hexagon orientation at a particular θ. Symbols: $\phi_A = 0.60$ (red circles), 0.68 (blue squares), 0.69 (black diamonds), 0.71 (green crosses), and 0.72 (pink plusses).

orientational order and quasi-long-range positional order, but only short-range molecular-orientational order. When $\phi_A > 0.68$, Ψ_6 and S_Δ are close to 1, and Φ_6 continues to increase and approaches to a saturation value ~0.6 as ϕ_A is increased to the maximum value obtained in the experiment. So for $\phi_A > 0.68$, the system is in a HX phase, in which not only the positions of hexagons but also the orientations of hexagons are ordered. In the HX phase, both $g_6(r)$ and $g_6{}^s(r)$ show strong correlations without detectable decays in the observed range of r (see examples at $\phi_A = 0.69$ and 0.72 in Fig. 3). Although plots of $g_6{}^{mo}(r)$ at $\phi_A = 0.69$ and 0.72 have lower magnitudes compared to unity, these functions do not show an apparent decay at large r. The absence of decays at large r indicate that in the HX phase bond-orientational order, positional order and molecular-orientational order are all (quasi-)long-range.

Structurally, there is no difference between HX and FHX phases, at least in terms of order parameters and correlation functions (see Supplemental Material, Fig. S1 [39]). To distinguish between the HX and FHX phases, movies showing the equilibrium fluctuating dynamics of the crowded hexagons are required. We reveal this distinction through our experiments by tracking the motion of hexagons and measuring time- and ensemble-averaged mean-square displacement (MSD) $\langle \Delta r^2(t) \rangle$ and mean-square angular displacement (MSAD) $\langle \Delta \theta^2(t) \rangle$ of hexagons, where t represents the time interval (Fig. 4). The ensemble size used for averaging is ~266–316 hexagons, and the time duration is about 5 min. In the RX phase (curves of $\phi_A = 0.60$ and 0.68 in Fig. 4), the translational motion of hexagons is confined near lattice points, as indicated by the plateau in MSD curves at long times. The magnitude of the plateau reflects the degree of confinement resulting from crowding by neighboring hexagons. MSAD curves in the RX phase, however, show no restriction and increase with t, indicating that hexagon rotation in the RX phase is not confined and particles can explore all angles. We show two examples of rotational trajectories, represented by circle and square symbols, in Fig. 4(c); given the sixfold symmetry of a hexagon particle, if the orientation of a hexagon can explore at least an angle range of $\pi/3$, then this particle is effectively considered to be able to explore all angles. Consequently, the histogram $p(\theta)$ in the RX phase shows a broad distribution over the entire angle range [Fig. 4(d)]. In the HX phase (curves of $\phi_A = 0.69$ in Fig. 4), hexagons become more restricted in translational motion as evidenced by the lower magnitude of the plateau in the MSD curve. Interestingly, for rotational motion, the MSAD curve shows a plateau at short times, but increases again at long times. This indicates a cagelike rotational behavior of hexagons, in which orientation of a hexagon fluctuates about a first value initially, then tip-tip passage occurs and the hexagon fluctuates a second different value (i.e., a rotational hopping occurs). An example of a rotational hopping trajectory is shown in Fig. 4(c) (see diamond symbols). $p(\theta)$ in the HX phase exhibits a narrow distribution with a single peak due to the uniform orientation of hexagons. To improve the statistics, $p(\theta)$ is measured in the angle range of $[0, \pi/3)$ using θ mod $\pi/3$ due to sixfold

symmetry of hexagons. So, in this case, rotational hopping of hexagons (i.e., tip-tip passage events) does not contribute much to $p(\theta)$, and did not show a second peak as observed in $p(\theta)$ of pentagons where the full range of θ is used. At even higher area fractions $\phi_A = 0.71$ and 0.72 (Fig. 4), both MSD and MSAD curves show plateaus with small magnitudes at long times, indicating that hexagons are tightly confined both in translation and in rotation, and rotational hopping is no longer observable over a readily accessible experimental timescale. At such high particle densities, such a rotational hopping event would require a collective motion of many particles (i.e., substantial local density fluctuation) in order to make enough room for one particle to hop rotationally. Such collective motion becomes extremely rare at high ϕ_A [see two examples of rotational trajectories represented by cross and plus symbols in Fig. 4(c)]. Therefore, we conclude based on experimental observations of dynamics that the system is in the FHX phase. Correspondingly, the single peak in $p(\theta)$ becomes more pronounced with an increased magnitude and a narrower width, indicating the reduced variability in hexagon orientation in the more tightly packed FHX phase. The HX-FHX rotational ergodic-nonergodic transition is continuous and the transition point will be likely shifted with the particle shape.

Our experimental observations reveal a richer crystal phase behavior compared with prior simulation results [24]. Specifically, our experimental system exhibits a hexagonal rotator crystal first and then a hexagonal crystal as ϕ_A increases. This indicates that the bond-orientational order is developed before the molecular-orientational order in our experimental system. This observation is different than simulation results which found that the molecular-orientational order and the bond-orientational order are closely correlated in solid phases, even in the highest density pure isotropic fluid phase [24]. Our observations also reveal the FHX phase at very high densities, which is distinguishable from the HX phase through analysis of hexagon dynamics, not structure. Anderson *et al.*'s reported phase behavior of a system consisting of perfect hexagons by MC simulations [24] includes a continuous two-step KTHNY melting: a continuous solid-to-hexatic phase transition and then a continuous hexatic-to-isotropic phase transition. However, given experimental limitations and the very narrow range in ϕ_A associated with the predicted existence of the hexatic phase, a definitive experimental identification of a hexatic phase of hexagons and its associated phase transitions cannot be conclusively made using our observations of rounded hexagons alone. Additional refinements to the experiments are needed in order to test with certainty regarding the possible existence of the hexatic phase, and this will be done in the future.

To go beyond the simulation work done by Anderson *et al.* [24] on perfect hexagons and investigate the effect of corner roundness on the phase behavior of hexagons, we have performed MC simulations of regular hexagons having different corner roundness ζ in isothermal-isobaric *NPT* ensembles (containing $N = 3584$ particles) in a square box with periodic boundary conditions. First, as a control study, we apply this simulation method to a system of perfect hexagons, and the results we obtained agree with those of Anderson *et al.* [24] (see more details in the Supplemental Material [39]). We then apply our MC simulation to rounded hexagons with $\zeta = 0.3$, and the results are shown in Fig. 2(b). We can see both RX and HX phases observed in experiments are recovered in MC simulations. However, the H-RX transition point obtained from the simulation is at $\phi_A = 0.713$, whereas in the experiment the I-RX transition point is at $\phi_A = 0.6$. There are several factors that could contribute to the difference between the simulated and experimentally observed area fractions associated with these transitions. One is the size polydispersity of hexagons used in experiments (∼6%). Another factor is the inherent nanoscale surface roughness on the edges of lithographic-fabricated hexagons, which could result in a bigger effective area (upper bound is estimated to be 6.8% more than the bare surface area). These two factors together give an effective area fraction $\phi_{A,\mathrm{eff}} \sim 0.64 \pm 0.08$ at I-RX transition measured in the experiment, which can account for the discrepancy between experiments and simulations. From the simulation aspect, the system size effect is a factor that needs to be considered. For our MC simulations, we have also used a smaller system consisting of 1840 particles, and the results show the area fraction at the H-RX transition is 0.711 for this smaller system, which is very close to the value 0.713 obtained for a system of 3584 particles (see Supplemental Material, Fig. S2 [39]). We can evaluate the system size effect by comparing ϕ_A at the H-RX transition for two systems: one is a system consisting of 3584 perfect hexagons used in this work and the other is a much bigger system consisting of 512^2 perfect hexagons employed by Anderson *et al.* [24]. The results show ϕ_A at the H-RX transition is 0.702 for the system of 3584 particles and 0.710 for the system of 512^2 hexagons [24], and thus the uncertainty in the area fraction due to the system size effect in simulations is estimated to be less than 1.5%.

We also find a hexatic phase for hexagons with $\zeta = 0.3$ in our MC simulations, although over a very small range of ϕ_A. Since in the experiments a tilted sample was used, in which there is a density gradient of particles along the tilting direction, the resulting limited spatial dynamic range of our experimental observations (particularly at intermediate densities) may mask the possible hexatic phase which is only stable over a very narrow range of ϕ_A between 0.695 and 0.713.

In the solid-crystal phase region, the simulation results show that Ψ_6 is already large when the system reaches the solid phase, and Ψ_6 approaches 1 steadily as ϕ_A increases. A similar trend is also found for S_Δ, although the saturation value of S_Δ is below 1 due to defects in the crystals. By contrast, Φ_6 starts from a much lower value of ∼0.25 when the simulation system first reaches the solid phase, and then increases with ϕ_A in an approximately linear way. So to clarify our boundary of the solid phase obtained in simulations, we set a threshold value of Φ_6 to be 0.5, which roughly corresponds to the value of Φ_6 at the RX-HX transition point obtained in experiments, and then for $0.713 < \phi_A < 0.786$, $\Phi_6 < 0.5$ and the system is in the RX phase, while for $\phi_A > 0.786$, $\Phi_6 > 0.5$ and the system is in the HX phase. If we rescale the MC simulation results by matching the H-RX transition point ($\phi_A = 0.713$) obtained from the simulation to the I-RX transition point ($\phi_A = 0.6$) measured in the experiment, then the rescaled $\phi_{A,\mathrm{rescaled}} = 0.66$ at RX-HX transition in the

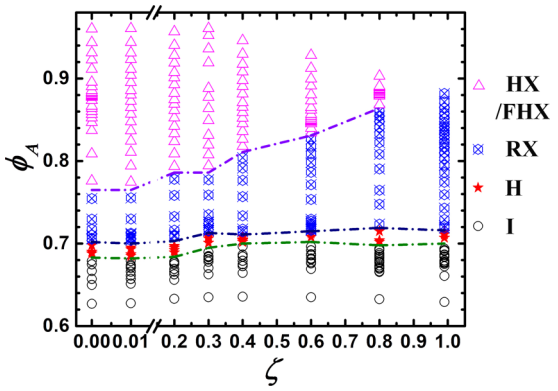

FIG. 5. Phase diagram of corner-rounded hexagons in the ϕ_A-ζ plane obtained by MC simulations of 3584 particles from expansion runs. $\zeta = 0$ corresponds to a perfect hexagon shape with ideally sharp vertices, and $\zeta = 0.99$ corresponds to a nearly disklike shape.

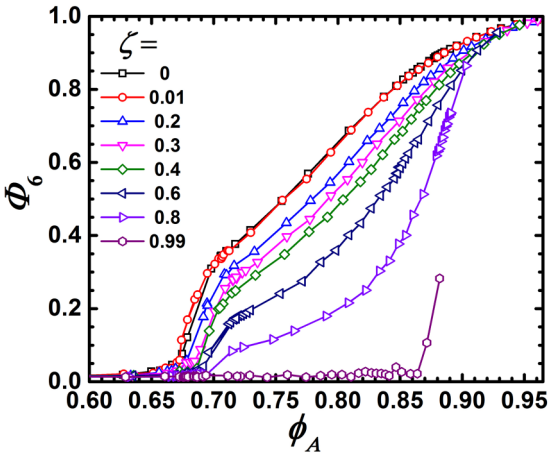

FIG. 6. Molecular-orientational order Φ_6 at different ϕ_A for hexagons with different corner-roundness ζ.

simulation also agrees with the one obtained in the experiment (i.e., 0.68). In both RX and HX phases of the simulation, $g_6(r)$ barely shows an algebraic decay at large r, and $g_6{}^s(r)$ shows a slow algebraic decay at large r with an exponent larger than $-1/3$. In contrast, $g_6{}^{\rm mo}(r)$ at large r remains at a low value in the RX phase and it gradually increases to a relatively large value in the HX phase (see Supplemental Material, Fig. S3 [39] for more details on order parameters and correlation functions). Overall, our rescaled simulation results agree reasonably well with our experimental observations for $\zeta = 0.3$. The slow increase of Φ_6 with ϕ_A also indicates that the RX-HX transition is continuous.

To develop a more complete understanding of the effect of corner roundness ζ on the phase behavior of rounded hexagons, we have systematically studied the phase behavior of corner-rounded hexagons by MC simulations. The obtained phase diagram of rounded hexagons is shown in Fig. 5 (see Supplemental Material and Supplemental Figs. S4–S11 for more details [39]). We can see that in all tested rounded hexagons, the hexatic phase is observed but at varied ranges of ϕ_A. The starting ϕ_A at which the hexatic phase appears is shifted upward as ζ increases (i.e., closer to a disklike shape). This agrees with the results shown by Anderson *et al.* that the starting ϕ_A of the hexatic phase of regular n-gons increases with n [24].

The effect of corner roundness on the molecular orientation of particles is shown in Fig. 6. We can see that under the same ϕ_A in the range of [0.68, 0.9], which mainly covers the RX and HX/FHX regions, Φ_6 decreases as ζ increases. In other words, the rounded hexagon particles have a greater capacity to become misaligned as ζ increases. This is understandable since hexagons with large ζ will behave more like a disk, and thus a more crowded packing is required in order for the allowed orientations of a given particle to be more strongly constrained by its neighbors. For a similar reason, the RX-HX phase transition shifts progressively to higher ϕ_A as ζ increases (shown in Fig. 5). In the limiting case of a disk shape, since there is no particular orientation that can be identified, Φ_6 essentially fluctuates around the noise level.

Among the regular n-gons, the observed phase behavior of crowded Brownian systems of polygons with $n \leqslant 5$ are all unique, as shown in prior experiments by Zhao and Mason [1,26–28]. This has also been seen by Anderson *et al.* in simulations which extended n up to 14 [24]. Experimentally, for systems of triangles, squares, and pentagons, none of these systems develops a spatially ordered phase with the same symmetry as the shape the constituent particle has when slowly crowded [26–28]. Systems of hard regular triangles do show a liquid-crystal "triatic" phase that exhibits fluctuating local chiral symmetry breaking, but this does not have long-range spatial order. A crowded system of hard Brownian hexagons, on the other hand, shows RX and HX phases which have the same sixfold symmetry as the hexagon shape. Rotational behavior (including hopping behavior) of regular n-gons in dense Brownian systems depends on n as well as on ζ.

To generalize the onset of nonergodicity in the rotations of n-gons, we develop a relatively simple geometrical model. We consider a freely rotating regular n-gon pinned at its center. Such a freely rotating n-gon will sweep out an area corresponding to the circle circumscribing the n-gon [Fig. 7(a)]. We calculate the area fraction $\phi_A{}^{\rm CD,hcp}$ at which the corresponding disk enclosed by the circumscribing circle of the n-gon reaches 2D hexagonal close packing [see an example for hexagons in Fig. 7(b)]. Then we can plot both $\phi_A{}^{\rm CD,hcp}$ and the lowest area fraction $\phi_A{}^{\rm R}$ (reported experimentally) at which n-gon rotation becomes nonergodic as a function of n [Fig. 7(c)]. For example, for triangles, $\phi_A{}^{\rm CD,hcp} = 0.375$, while the lowest area fraction, $\phi_A{}^{\rm R}$ is 0.55, at which the triangle system exhibits a triatic phase and the rotation of triangles is restricted and becomes nonergodic [28]. Similarly, for squares, particle rotation becomes nonergodic at $\phi_A{}^R = 0.66$ in a RB phase [27], while for pentagons and hexagons, the rotational ergodic-nonergodic transition happens roughly at $\phi_A{}^{\rm R} = 0.75$ and 0.71, respectively. These area fractions correspond to the FRX phase in the pentagon system [26], and the FHX phase in the hexagon system. We can see that in order to restrict the rotation of polygons, a higher $\phi_A{}^{\rm R}$ than $\phi_A{}^{\rm CD,hcp}$ is needed so that tip-tip passages will be hindered. In addition, Fig. 7(c) also shows that as n of a regular n-gon increases (i.e., approaches a disk), the difference between $\phi_A{}^{\rm R}$ and $\phi_A{}^{\rm CD,hcp}$ is reduced. We should note that this simple geometrical model

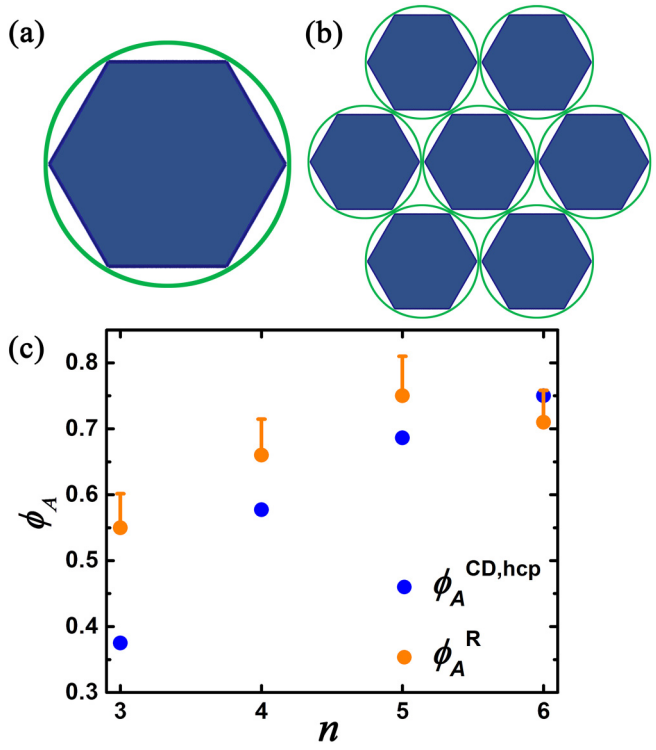

FIG. 7. (a) Illustration of the circumscribed circle touching the vertices of a regular hexagon. (b) Schematic showing one example of hexagons when their circumscribed circles are close packed. (c) The area fractions $\phi_A{}^{CD,hcp}$ and $\phi_A{}^{R}$ as a function of n for regular n-gons. $\phi_A{}^{CD,hcp}$ is the area fraction of n-gons when their circumscribed circles are at closest packing, which is obtained by $\phi_A{}^{CD,hcp} = \frac{n}{2\pi}\sin(\frac{2\pi}{n}) \times \frac{\pi}{2\sqrt{3}}$, where the first factor is the area ratio of n-gon and its circumscribed circle, and the second factor is the closest packing density of disks; $\phi_A{}^{R}$ is the observed area fraction at which n-gon rotation in a dense Brownian system becomes nonergodic. For triangles ($n = 3$), $\phi_A{}^{R} = 0.55$ and the triangle system is in a triatic phase [28]; for squares ($n = 4$), $\phi_A{}^{R} = 0.66$ and the square system is in a rhombic crystal phase [27]; for pentagons ($n = 5$), $\phi_A{}^{R} = 0.75$ and the pentagon system is in a FRX phase [26]; while for hexagons ($n = 6$), $\phi_A{}^{R} = 0.71$ and the hexagon system is in a FHX phase. The error bars indicate the upper bound of the expected possible increase in the effective ϕ_A of each regular polygon due to edge roughness.

does not capture fluctuations of positions and orientations of surrounding polygons that are no doubt present in the real experimental system. These fluctuations would lead to a range of possible angles of center polygons, and even dynamical heterogeneity in rotations, especially for area fractions near the rotational ergodic-nonergodic transition point. Interestingly, the fact that rotational ergodic-nonergodic transitions happen in phases with different translational order for different n-gons indicates a different coupling between translational and rotational motion of particles in those systems, which would be worth studying in future work.

IV. CONCLUSIONS

In this work, we have studied the phase behavior of rounded hexagons both by experiments and by MC simulations. Compared to earlier simulation work, our experimental results reveal a much richer phase behavior in the solid-crystal region. We find that in the crystal region, RX is formed first at low ϕ_A, and then HX is observed as the orientation of hexagons becomes uniform at high ϕ_A. At even higher ϕ_A, the crowding of particles greatly restricts the rotation of hexagons, and results in a structurally similar but dynamically different phase FHX. All those crystal phases have the same sixfold symmetry as the regular hexagon shape has. This is different from earlier experimental observations on regular triangles, squares, and pentagons, whose assembled ordered structures in the surface fraction range explored experimentally did not show the rotational symmetries of the shapes of constitutent particles. Our MC simulations on rounded hexagons confirm the RX-HX transition and reveal that the molecular-orientational order in the crystal phase gradually decreases with increasing corner roundness, indicating that the coupling between particles rotation and particles translation is reduced as particles become more rounded. It will be also interesting for a future work to apply a simulation method in which the dynamics can be revealed to see the HX-FHX transition that we have identified through experiments. The findings in this study provide insights in controlling self-assembly of colloids through appropriate particle shape-design.

ACKNOWLEDGMENTS

This work is supported by the National Natural Science Foundation of China (Grants No. 21573159 and No. 11874277), Open Project of State Key Laboratory for Supramolecular Structure and Materials (Grant No. SKLSSM2015028) and High Performance Computing Center of Tianjin University. T.G.M. acknowledges financial support from UCLA. The work was carried out at the National Supercomputer Center in Tianjin, and the calculations were performed on TianHe-1(A).

[1] K. Zhao and T. G. Mason, Assembly of colloidal particles in solution, Rep. Prog. Phys. **81**126601 (2018).
[2] G. M. Whitesides and B. A. Grzybowski, Self-assembly at all scales, Science **295**, 2418 (2002).
[3] S. C. Glotzer, Some assembly required, Science **306**, 419 (2004).
[4] S. C. Glotzer and M. J. Solomon, Anisotropy of building blocks and their assembly into complex structures, Nat. Mater. **6**, 557 (2007).
[5] L. Onsager, The effects of shape on the interaction of colloidal particles, Ann. NY Acad. Sci. **51**, 627 (1949).
[6] M. E. Leunissen, C. G. Christova, A. P. Hynninen, C. P. Royall, A. I. Campbell, A. Imhof, M. Dijkstra, R. van Roij, and A. van Blaaderen, Ionic colloidal crystals of oppositely charged particles, Nature (London) **437**, 235 (2005).
[7] J. Zhang, E. Luijten, and S. Granick, Toward design rules of directional Janus colloidal assembly, Annu. Rev. Phys. Chem. **66**, 581 (2015).

[8] K. Zhao and T. G. Mason, Directing Colloidal Self-Assembly Through Roughness-Controlled Depletion Attractions, Phys. Rev. Lett. **99**, 268301 (2007).

[9] K. Zhao and T. G. Mason, Suppressing and Enhancing Depletion Attractions Between Surfaces Roughened by Asperities, Phys. Rev. Lett. **101**, 148301 (2008).

[10] W. B. Russel, D. A. Saville, and W. R. Schowalter, *Colloidal Dispersions* (Cambridge University Press, Cambridge, 1989).

[11] E. P. Bernard and W. Krauth, Two-Step Melting in Two Dimensions: First-Order Liquid-Hexatic Transition, Phys. Rev. Lett. **107**155704 (2011).

[12] M. Engel, J. A. Anderson, S. C. Glotzer, M. Isobe, E. P. Bernard, and W. Krauth, Hard-disk equation of state: First-order liquid-hexatic transition in two dimensions with three simulation methods, Phys. Rev. E **87**, 042134 (2013).

[13] J. M. Kosterlitz and D. J. Thouless, Ordering, metastability and phase transitions in two-dimensional systems, J. Phys. C: Solid State Phys. **6**, 1181 (1973).

[14] B. I. Halperin and D. R. Nelson, Theory of Two-Dimensional Melting, Phys. Rev. Lett. **41**, 121 (1978).

[15] A. P. Young, Melting and the vector Coulomb gas in two dimensions, Phys. Rev. B **19**, 1855 (1979).

[16] M. A. Bates and D. Frenkel, Phase behavior of two-dimensional hard rod fluids, J. Chem. Phys. **112**, 10034 (2000).

[17] J. Vieillard-Baron, Phase transitions of the classical hard-ellipse system, J. Chem. Phys. **56**, 4729 (1972).

[18] D. Frenkel, Soft condensed matter, Physica A **313**, 1 (2002).

[19] M. Benedict and J. F. Maguire, Molecular dynamics simulation of nanomaterials using an artificial neural net, Phys. Rev. B **70**, 174112 (2004).

[20] K. W. Wojciechowski and D. Frenkel, Tetratic phase in the planar hard square system, Comput. Methods Sci. Technol. **10**, 235 (2004).

[21] T. Schilling, S. Pronk, B. M. Mulder, and D. Frenkel, Monte Carlo study of hard pentagons, Phys. Rev. E **71**, 036138 (2005).

[22] A. Donev, J. Burton, F. H. Stillinger, and S. Torquato, Tetratic order in the phase behavior of a hard-rectangle system, Phys. Rev. B **73**, 054109 (2006).

[23] C. Avendano and F. A. Escobedo, Phase behavior of rounded hard-squares, Soft Matter **8**, 4675 (2012).

[24] J. A. Anderson, J. Antonaglia, J. A. Millan, M. Engel, and S. C. Glotzer, Shape and Symmetry Determine Two-Dimensional Melting Transitions of Hard Regular Polygons, Phys. Rev. X **7**, 021001 (2017).

[25] Z. L. Hou, Y. Ju, Y. W. Zong, F. F. Ye, and K. Zhao, Molecular dynamics simulations on the dynamics of two-dimensional rounded squares, Chin. Phys. B **27**, 088203 (2018).

[26] K. Zhao and T. G. Mason, Frustrated Rotator Crystals and Glasses of Brownian Pentagons, Phys. Rev. Lett. **103**, 208302 (2009).

[27] K. Zhao, R. Bruinsma, and T. G. Mason, Entropic crystal-crystal transitions of Brownian squares, Proc. Natl. Acad. Sci. USA **108**, 2684 (2011).

[28] K. Zhao, R. Bruinsma, and T. G. Mason, Local chiral symmetry breaking in triatic liquid crystals, Nat. Commun. **3**, 801 (2012).

[29] K. Zhao and T. G. Mason, Twinning of rhombic colloidal crystals, J. Am. Chem. Soc. **134**, 18125 (2012).

[30] K. Mayoral and T. G. Mason, Entropic chiral symmetry breaking in self-organized two-dimensional colloidal crystals, Soft Matter **10**, 4471 (2014).

[31] K. Zhao and T. G. Mason, Self-organized chiral colloidal crystals of Brownian square crosses, J. Phys. Condens. Matter **26**, 152101 (2014).

[32] L. Rossi and T. G. Mason, Controlling enantiomeric populations in fluctuating Brownian monolayers of chiral colloids, Soft Matter **11**, 2461 (2015).

[33] K. Zhao and T. G. Mason, Shape-designed frustration by local polymorphism in a near-equilibrium colloidal glass, Proc. Natl. Acad. Sci. USA **112**, 12063 (2015).

[34] F. C. Bawden, N. W. Pirie, J. D. Bernal, and I. Fankuchen, Liquid crystalline substances from virus-infected plants, Nature (London) **138**, 1051 (1936).

[35] S. Sacanna and D. J. Pine, Shape-anisotropic colloids: Building blocks for complex assemblies, Curr. Opin. Colloid Interface Sci. **16**, 96 (2011).

[36] A. B. Brown, C. G. Smith, and A. R. Rennie, Fabricating colloidal particles with photolithography and their interactions at an air-water interface, Phys. Rev. E **62**, 951 (2000).

[37] C. J. Hernandez and T. G. Mason, Colloidal alphabet soup: Monodisperse dispersions of shape-designed LithoParticles, J. Phys. Chem. C **111**, 4477 (2007).

[38] K. Zhao, C. G. A. Harrison, D. A. Huse, W. B. Russel, and P. M. Chaikin, Nematic and almost-tetratic phases of colloidal rectangles, Phys. Rev. E **76**, 040401 (2007).

[39] See Supplemental Material at http://link.aps.org/supplemental/10.1103/PhysRevMaterials.3.015601 for more details.

[40] D. R. Nelson, *Defects and Geometry in Condensed Matter* (Cambridge University Press, Cambridge, 2002).